Damage-Induced Acceleration of Molten Salt Corrosion in Ni-Coated Alloys

Younghwan Jeon[a], Kyeongtae Park [b], Jaeyeong Park[b*]
[a]Advanced Fuel Cycle Technology Division, Korea Atomic Energy Research Institute,
111, Daedeok-daero 989beon-gil, Yuseong-gu, Daejeon, 34057, Republic of Korea
[b]Department of Nuclear Engineering, Ulsan National Institute of Science and Technology,
50 UNIST-gil, Ulju-gun, Ulsan 44919, Republic of Korea
[*]Corresponding author: jypark@unist.ac.kr

***Keywords :** Ni-coating, Molten salt, Molten salt reactor, Electrochemistry, Pitting, Crevice

1. Introduction

The molten salt reactor (MSR), recognized as a promising Generation IV nuclear reactor system, utilizes molten salts that simultaneously function as both primary coolant and fissile fuel carrier, exhibiting inherent safety characteristics, high thermal efficiency, and design compactness. Global research initiatives, including Korea's focused development of chloride-based MSR configurations, highlight its technological potential. Critical research domains span neutronics optimization, reactor architecture design, multiphase thermal-fluid dynamics, and thermophysical property characterization of salt mixtures.

A principal technological barrier in MSR implementation involves material degradation through molten salt corrosion, driven by multiple mechanisms: electrochemical redox processes ($2U^{4+} + Cr \rightarrow 2U^{3+} + Cr^{2+}$), oxidative attack from hygroscopic/oxygen impurities, and reactive fission product interactions. Contemporary mitigation methodologies employ salt purification protocols, fission product sequestration techniques, and electrochemical potential modulation via sacrificial metal introduction or uranium valence state control. While these strategies demonstrate partial corrosion attenuation, complete prevention remains technically unattained.

Material compatibility studies reveal superior molten salt corrosion resistance in pure nickel relative to conventional Ni-based alloys, though its structural limitations and atmospheric oxidation susceptibility restrict engineering applications. This investigation systematically examines nickel-clad alloy systems through multi-scenario corrosion testing, combining metallurgical analysis with operational parameter variation to assess their viability as structural materials under MSR service conditions.

2. Methods and Results

2.1 Specimen Preparation

Five distinct corrosion specimen categories were fabricated: Ni-based alloy (80Ni–20Cr), pure Ni, Ni-coated Ni-based alloy, intentionally damaged Ni-coated Ni-based alloy, and partially Ni-coated Ni-based alloy. The Ni-based alloy and pure Ni substrates were precision-machined via electrical discharge machining (EDM) and subsequently polished to a 2000-grit finish prior to experimental procedures or coating deposition. The specimen geometry is illustrated in Fig. 1 (a).

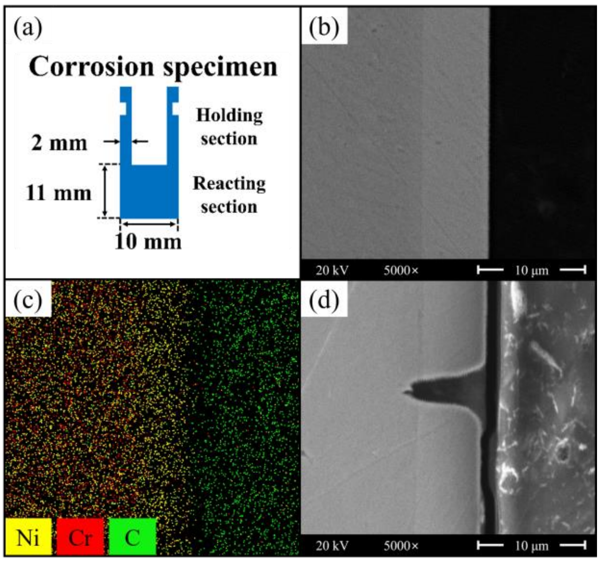

Fig. 1. Schematic representation of corrosion specimen (a), cross-sectional SEM–EDS micrographs of Ni-coated Ni-based alloy (b, c), and cross-sectional SEM image of intentionally damaged Ni-coated Ni-based alloy (d)

Ni coating was electrodeposited from an aqueous electrolyte containing 250 g L^{-1} $NiSO_4{\cdot}6H_2O$, 35 g L^{-1} H_3BO_3, and 40 g L^{-1} $NiCl_2{\cdot}6H_2O$, with pH adjusted to 3.5 using ammonia solution. Deposition parameters were maintained at 6 mA cm^{-2} for 2580 seconds at 55 °C, yielding a nominal 5 μm Ni layer thickness (Fig. 1 (b, c)). Partially coated specimens were produced by masking with conductive Cu tape prior to deposition. Intentionally damaged specimens were subjected to focused ion beam (FIB) milling to generate three micro-cracks (500 μm × 3 μm × 7 μm) per specimen (Fig. 1 (d)).

2.2 Corrosion Cell Configuration

Salt preparation and corrosion experiments were conducted in an Ar-filled glove box with moisture and oxygen levels rigorously maintained below 0.1 ppm. High-purity NaCl and $MgCl_2$ (both Alfa Aesar, 99.99%) underwent stepwise thermal treatment at 200 ℃, 400 ℃, and 600 ℃ for 24 hours each to minimize residual moisture and oxygen content before being mixed to the eutectic composition (58.0 at% NaCl–42.0 at% $MgCl_2$). A cylindrical boron nitride (BN) crucible (30 mm inner diameter) contained 15.000 g of the salt mixture for each experiment. Specimen immersion depth was carefully controlled to ensure full submersion of the reactive section while limiting exposure of the connecting section to less than 1 mm.

Corrosion experiments were conducted at 700 ℃, with temperature regulation provided by a PID-controlled electrical furnace. A centrally positioned dummy cell filled with NaCl–$MgCl_2$ enabled continuous temperature monitoring and verification throughout the experimental duration. Post-experiment, the corrosion cell was rapidly withdrawn to prevent salt solidification, facilitating specimen extraction and salt separation from the BN crucible.

2.3 Experimental Methodology

Corrosion experiments were performed on the five specimen types for durations of 3, 7, 14, and 21 days (Table I). Pre-experiment specimen preparation involved ethanol cleaning, vacuum drying, and precise mass determination using an analytical balance. Post-experiment, specimens underwent ultrasonic cleaning in deionized water for 200 minutes, followed by vacuum drying and mass measurement to quantify corrosion-induced weight changes. Approximately 0.2 g of pulverized salt from each experiment was analyzed via ICP-OES to determine alloying element content.

Table I. Experimental matrix for corrosion studies

Test ID	Corrosion duration	Note
S-3	3 days	Un-coated 80Ni–20Cr
S-7	7 days	
S-14	14 days	
S-21	21 days	
N-3	3 days	Pure Ni
N-7	7 days	
N-14	14 days	
N-21	21 days	
C-3	3 days	5 μm-Ni-coated 80Ni–20Cr
C-7	7 days	
C-14	14 days	
C-21	21 days	
D-3	3 days	Ni-coated 80Ni–20Cr with 3 micro-cracks
D-7	7 days	
D-14	14 days	
D-21	21 days	
H-3	3 days	Half Ni-coated 80Ni–20Cr
H-7	7 days	
H-14	14 days	
H-21	21 days	

Microstructural evolution was characterized through SEM–EDS analysis of specimen surfaces and cross-sections. Cross-sectional samples were prepared by precision cutting, vertical mounting in embedding clips on graphite substrates, and metallographic polishing culminating in a 1 μm Al_2O_3 suspension finish. For damaged Ni-coated specimens (Test ID: D), controlled material removal during polishing enabled targeted observation of FIB-induced cracks.

3. Results

3.1 Mass Loss and Salt Contaminant Analysis

Post-corrosion mass variations and quantified Ni and Cr concentrations in molten salt are summarized in Fig. 2 (a), with normalized corrosion rates relative to uncoated Ni-based alloy (Test ID: S) illustrated in Fig. 2 (b). Specimens exhibited a hierarchical corrosion resistance profile ordered as: N (pure Ni) > C (intact Ni coating) > D (micro-cracked coating) > H (half-coated) > S (uncoated). ICP-OES analysis revealed undetectable Ni dissolution in uncoated specimens (S-series), whereas trace Ni dissolution (<1 ppm) occurred in C, D, and H specimens. Notably, Ni concentrations in C and D specimens decreased at 14–21 days compared to 3–7 days, suggesting time-dependent interfacial phenomena. Corrosion rates for C and D specimens remained below 20% and 25%, respectively, during initial exposure ($\leq$ 7 days), but escalated to 35% and 40% after 14 days.

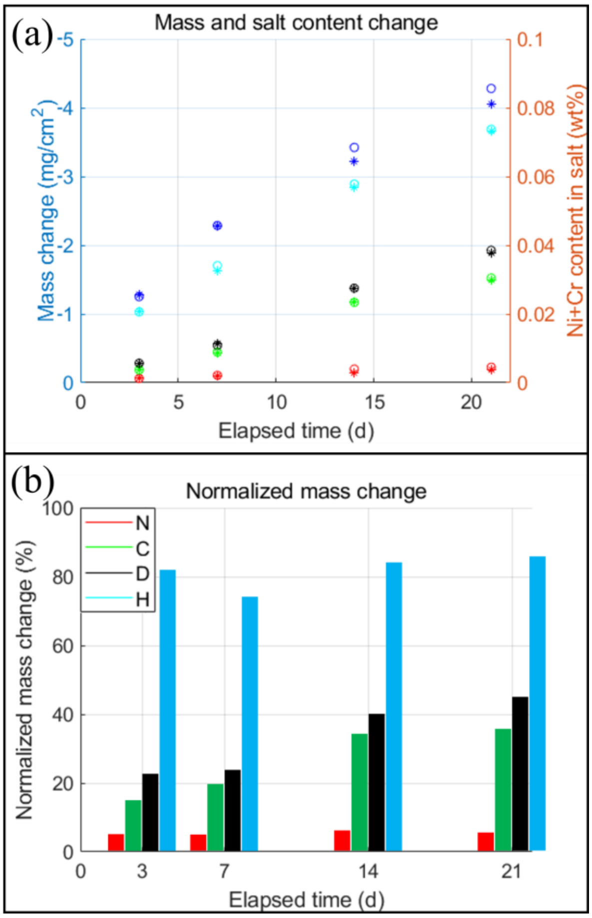

Fig. 2. Temporal mass variation and salt-phase alloying element concentrations; (b) Normalized corrosion rates relative to uncoated Ni-based alloy

3.2 Microstructural Degradation Analysis

Cross-sectional SEM–EDS of S-21 (uncoated) and N-21 (pure Ni) specimens (Fig. 3) demonstrated superior corrosion resistance of pure Ni, with mass loss rates 90% lower than 80Ni–20Cr alloy. Intact Ni-coated specimens (C-series) exhibited preferential Ni-layer dissolution, effectively shielding the substrate (Fig. 4 (a)). However, prolonged exposure (C-21) resulted in coating perforation and subsequent substrate corrosion (Fig. 4 (b)).

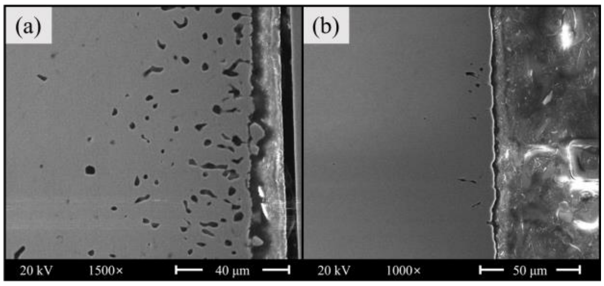

Fig. 3. ross-sectional micrographs: (a) Severe intergranular attack in S-21; (b) Minimal surface recession in N-21

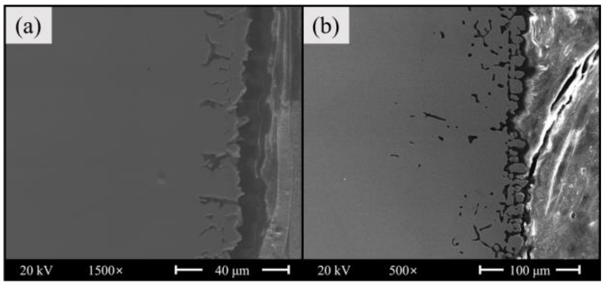

Fig. 4. Coating integrity effects: (a) Localized Ni-layer dissolution in C-7; (b) Coating failure and substrate penetration in C-21

Micro-cracked specimens (D-series) developed subsurface pitting corrosion beneath artificial defects (Fig. 5), with pit volume expanding proportionally to exposure duration. Half-coated specimens (H-series) exhibited crevice corrosion at coating-substrate interfaces (Fig. 6), where uncovered regions experienced deeper corrosion penetration than coated zones.

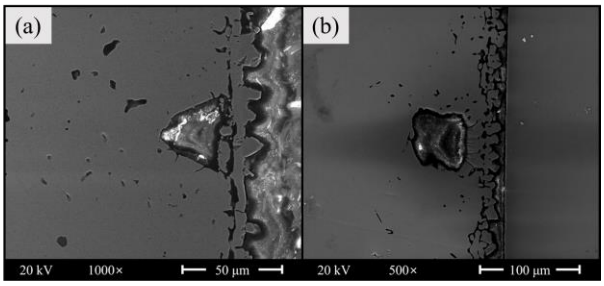

Fig. 5. Micro-crack-induced pitting evolution: (a) Incipient pit formation in D-14; (b) Mature pit morphology in D-21

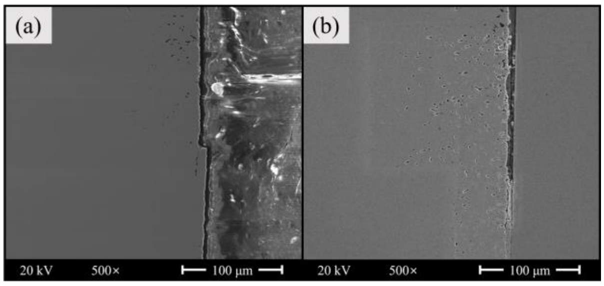

Fig. 6. Interface-driven degradation: (a) Crevice initiation in H-7; (b) Accelerated interfacial attack in H-21

4. Discussion

3.2 Coating Efficacy and Failure Modes

Intact Ni coatings reduced corrosion rates by 75–80% compared to uncoated substrates, validating their protective capacity. However, coating breach via either artificial defects (D-series) or edge exposure (H-series) eliminated this advantage, inducing localized corrosion rates exceeding 120% of baseline. Calculated Ni-layer dissolution rates (25–26 μm yr^{-1}) suggest a minimum 300 μm coating thickness requirement for decade-scale structural integrity under operational conditions.

4.2 Electrochemical and Interfacial Dynamics

Ni particulate deposition on coated specimens and time-dependent Ni dissolution trends are attributed to redox equilibria between Ni^{2+} ions and Cr ($Ni^{2+}+Cr \rightarrow Ni^{0}+Cr^{2+}$). In damaged coatings, rapid Ni^{2+}–Cr interactions at exposed interfaces generated localized potential gradients, driving pitting and crevice corrosion. The observed Ni concentration decrease in later-stage C specimens correlates with Cr oxidation saturation and passivation layer destabilization.

5. Conclusions

This work establishes that defect-free Ni coatings significantly mitigate molten salt corrosion (≤ 20% baseline rate) in chloride media. However, mechanical or corrosion-induced coating breaches precipitate localized degradation mechanisms (pitting/crevice corrosion) previously unreported in MSR material studies. These findings necessitate a dual design strategy: (1) optimization of coating thickness (>800 μm) for long-term protection and (2) implementation of crack-resistant coating architectures to prevent localized failure modes. The identified failure mechanisms provide critical input for next-generation corrosion-resistant alloy development in molten salt reactor systems.

Acknowledgment

This work was supported by the Molten Salt Reactor Development Agency grant funded by the Korea government (the Ministry of Science and ICT) [Project Number: RS-2023-00261146]

REFERENCES

[1] R. Roper, M. Harkema, P. Sabharwall, C. Riddle, B. Chisholm, B. Day, P. Marotta, Molten salt for advanced energy applications: A review, Annals of Nuclear Energy, Vol. 169, p. 108924, 2022.
[2] J. Zhang, C.W. Forsberg, M.F. Simpson, S. Guo, S.T. Lam, R.O. Scarlat, F. Carotti, K.J. Chan, P.M. Singh, W. Doniger, Redox potential control in molten salt systems for corrosion mitigation, Corrosion Science, Vol. 144, pp. 44-53, 2018.
[3] V. Afonichkin, A. Bovet, V. Shishkin, Salts purification and voltammetric study of the electroreduction of U (IV) to U (III) in molten LiF–ThF4, Journal of nuclear materials, Vol. 419, pp. 347-352, 2011.
[4] O. Beneš, E. Capelli, N. Morelová, J.-Y. Colle, A. Tosolin, T. Wiss, B. Cremer, R. Konings, Cesium and iodine release from fluoride-based molten salt reactor fuel, Physical Chemistry Chemical Physics, Vol. 23, pp. 9512-9523, 2021.
[5] L. Chen, L.-Y. He, B. Zhou, G.-F. Zhu, Y.-H. Fan, H.-J. Xu, R. Yan, Y. Zou, Evaluation on 131I production based on molten salt reactor off-gas extraction, Annals of Nuclear Energy, Vol. 195, p. 110192, 2024.
[6] H. Jin, Y.-Y. Wang, Y.-T. Wang, H.-B. Yang, Synthesis and properties of electrodeposited Ni–CeO 2 nano-composite coatings, Rare Metals, Vol. 37, pp. 148-153, 2018.
[7] A. Rashidi, A. Amadeh, Effect of electroplating parameters on microstructure of nanocrystalline nickel coatings, Journal of Materials Science & Technology, Vol. 26, pp. 82-86, 2010.